IEEE Access
Multidisciplinary : Rapid Review : Open Access Journal

Received 12 April 2024, accepted 30 April 2024, date of publication 3 May 2024, date of current version 10 May 2024.

Digital Object Identifier 10.1109/ACCESS.2024.3396575

RESEARCH ARTICLE

Noise-Robust Online Measurement of the On-State Resistance of the Power Semiconductor Devices in PWM Converters

JUNHO SHIN [1], JONG-WON SHIN [2], (Senior Member, IEEE), AND WONHEE KIM [3], (Member, IEEE)

[1]Department of Smart Cities, Chung-Ang University, Seoul 06974, South Korea
[2]Department of Electrical and Computer Engineering, Seoul National University, Seoul 08826, South Korea
[3]School of Energy Systems Engineering, Chung-Ang University, Seoul 06974, South Korea

Corresponding author: Jong-Won Shin (jongwonshin@snu.ac.kr)

This work was supported in part by the Research and Development Program of Korea Institute of Energy Research under Grant C3-2426, in part by the National Research Foundation of Korea (NRF) funded by the Ministry of Science and Information and Communication Technology (ICT) under Grant RS-2023-00217270, and in part by the Chung-Ang University Graduate Research Scholarship in 2022.

ABSTRACT The increase in R_{DUT}, the on-state resistance of power semiconductor devices, is used to estimate the remaining useful life (RUL) of the devices. Conventional online measurement of R_{DUT} involves on-state voltage measurement of the on-state device, which is easily polluted by switching noise to limit the measurement accuracy. This paper proposes a new noise-robust method to measure the increment of R_{DUT} by inductor current and input/output DC voltage of DC-DC converters. The proposed method features higher accuracy in predicting RUL than the conventional one because the inductor current is immune to switching noise. The aging of MOSFET is emulated in this paper by adding a series resistor R_{ext}. Experiments showed that the resistance increment measured by the proposed method is up to 99.2% accurate to value of R_{ext}.

INDEX TERMS On-state resistance, remaining useful life (RUL), online monitoring, power semiconductor devices.

I. INTRODUCTION

Power semiconductor devices such as metal oxide semiconductor field effect transistors (MOSFETs), insulated gate bipolar transistors (IGBTs), and diodes are identified as the most failure-prone components in power conversion systems (PCS) [1], [2]. Studies have been conducted to estimate the remaining useful life (RUL) of power semiconductors in PCS such as inverters and to use different control methods to increase the RUL [3]. As such, predicting the RUL of these devices is critical for avoiding failures and improving reliability of the PCS. The failures of power semiconductors have been analyzed and their predictive models have been studied to forecast the RUL [2]. The aging of IGBTs is predicted by changes in resonance characteristics [4] and gate-source voltage waveforms [5] in their off-state. This method does not require measuring other parameters, such as the current flowing through the power semiconductors, to determine aging. Estimating RUL from the changes in resonance and gate-source waveforms has disadvantage of requiring human verification with an instrument such as an oscilloscope.

The RUL of the power semiconductor devices is generally represented by their on-state resistances R_{DUT}, because the bond wires inside the package are gradually lifted off or cracked as they age [6], [7], [8], [9], [10], [11], [12], [13], [14]. One of the simplest ways to measure R_{DUT} is to use a multimeter or milli-ohm meter which is widely utilized to measure resistances. These meters, however, are not applicable to online measurement, i.e., measuring R_{DUT} while PCS is processing power, since they may be damaged by the high voltages and currents. Also, typical duration of the

The associate editor coordinating the review of this manuscript and approving it for publication was Ahmed Aboushady.

© 2024 The Authors. This work is licensed under a Creative Commons Attribution-NonCommercial-NoDerivatives 4.0 License. For more information, see https://creativecommons.org/licenses/by-nc-nd/4.0/

ON state of power semiconductor devices a few or a few tens of microseconds. The meters cannot measure R_{DUT} in this short interval due to their limited bandwidth. In addition, multimeters and milli-ohm meters measure the absolute value of the resistance, while the proposed method detects the increase in resistance – this point will be discussed in detail in the rest of the paper. Digital twin method analyzes the voltage and current dynamics of the operating PCS in real time [15], and is applicable to estimate the change in R_{DUT}. This approach is capable of observing multiple quantities simultaneously. However, the digital twin method may not be cost-effective compared to the circuit-based approach since it requires many sensors, high-rate data sampling which is higher enough than the switching frequency of PCS, and substantial computational resources.

A typical method of measuring R_{DUT} during the PCS operation is to sense the on-state voltage and on-state current of the power semiconductor device to calculate R_{DUT}. Fig. 1 represents the concept of conventional on-state voltage measurement circuit (OVMC) with a MOSFET as DUT (device under test). The OVMC measures the drain-source voltage of the DUT, v_{ds}, to estimate its RUL. The output voltage of the OVMC v_{out} is expressed as (1)

$$v_{out} = k_v (v_{ds} + v_n) \tag{1}$$

where k_v represents the total sensing gain of the OVMC and analog-to-digital converter (ADC) of microcontroller unit (MCU). Voltage v_n is the error by the switching noise which degrades the accuracy of the monitoring R_{DUT}. The output of the current sensor i_{out} is defined similarly as in (2).

$$i_{out} = k_i (i_{ds} + i_n) \tag{2}$$

In (2), k_i, i_{ds}, and i_n are the total sensing gain of the current sensor and the ADC, current flowing through the DUT, and current error by the switching noise. Because the current is generally less susceptible to the noise compared to the voltage, i_n is assumed zero or $i_n \cong 0$. Ohm's law provides the relationship between i_{ds}, v_{ds}, and R_{DUT} as in (3).

$$v_{ds} = i_{ds} R_{DUT} \tag{3}$$

Substituting (1) and (2) into (3) yields the expression of R_{DUT} in (4).

$$R_{DUT} = \frac{k_i}{k_v}\left(\frac{v_{out}}{i_{out}}\right) - \left(\frac{k_i}{i_{out}}\right) v_n \tag{4}$$

One representative drawback of the conventional OVMCs is that monitoring v_{ds} is highly prone to switching noise, i.e., v_n in (1) and (4) is not negligible. Since the MCU realizes the calculation of the right-hand side in (4) without filtering or correcting v_n, v_n distorts the value of R_{DUT} and thus degrades the accuracy of estimating the RUL of the DUT.

This paper proposes the monitoring technique of R_{DUT} of the working MOSFET without sensing or measuring the noise-sensitive v_{ds} [27]. This enhances the noise robustness of the estimation of RUL and simplifies the structure of the sensing circuit. Section II introduces the traditional OVMC structures and the limitations of conventional on-state resistance measurement methods. A comparison between the conventional OVMCs and the proposed method is explained in detail in Section III. The experimental setups and results are shown in Section IV, and the conclusion is discussed in Section V.

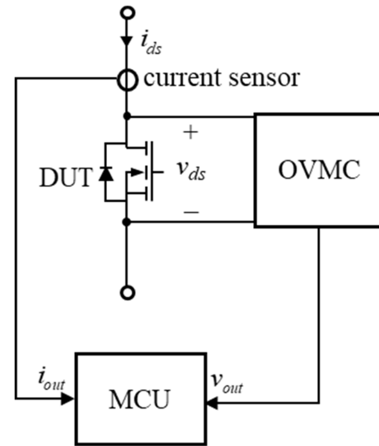

FIGURE 1. Conventional OVMC with a MOSFET as a DUT.

II. LIMITATION OF CONVENTIONAL ON-STATE RESISTANCE MEASUREMENT METHODS

Conventional OVMCs can be categorized into two: the one is to use diode clamp circuits [18], [19], [20], [21], [22], [23], [24], [25], [26], and the other is to utilize MOSFET clamp circuits [9], [10], [11], [16], [17]. The diode clamp circuits are again divided into two groups: the one using single diode [18], [19], [20], and the other using two series-connected diodes [21], [22], [23], [24], [25], [26]. This categorization is based on the number of forward-biased diodes excluding Zener diodes when the power semiconductor device is ON. The single diode clamping circuits sense on-state current. Circuit in [19] senses voltage across a resistor which is series-connected in the on-state current path. Circuits in [18], [20], and [21] detects the voltage across gallium nitride transistors. A clamp circuit using two diodes is used to analyze the aging of power semiconductors by power cycle [22] and thermal cycle [23]. The loss breakdown models and a calorimetric switching loss measurement method utilizing a two-diodes clamp circuit are presented in [25]. The simple OVMC using protection diode only [26] is free from the errors induced by diode, while its usage is limited from high-voltage applications.

Fig. 2(a) shows the representative single diode clamp circuit. Literals v_{gs}, v_{ds}, and i_{ds} are the gate-source voltage, drain-source voltage, and drain-source current of the DUT, respectively.This circuit has been widely used to sense the on-state current of MOSFETs or IGBTs since its simple structure without extra voltage source [28]. Utilizing the output voltage of the OVMC, v_{sen}, the estimation of the RUL was conducted as well [29]. The operation is as follows: clamp

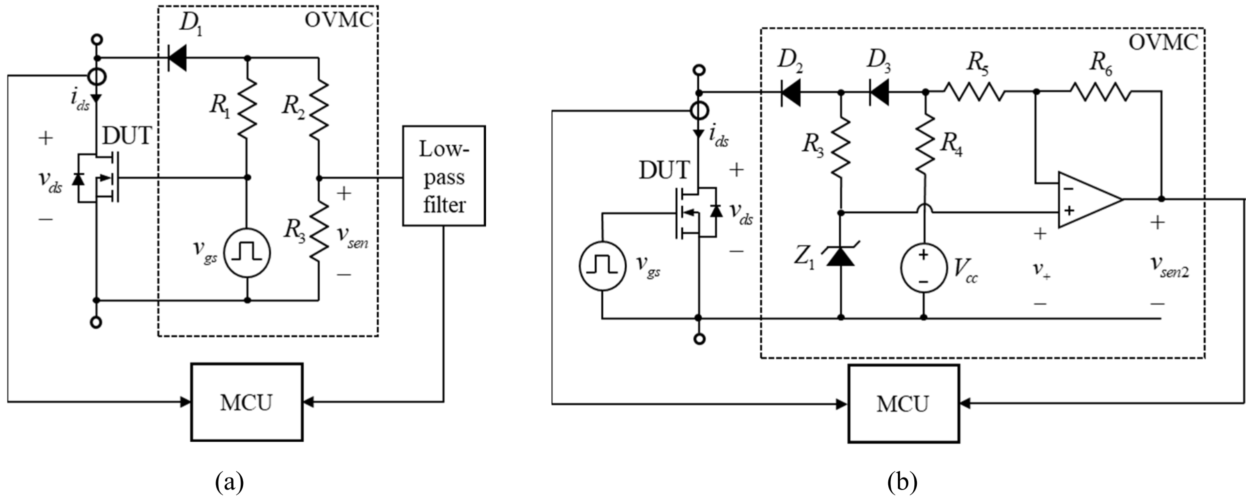

FIGURE 2. Conventional OVMCs based on (a) single clamp diode and (b) two diodes.

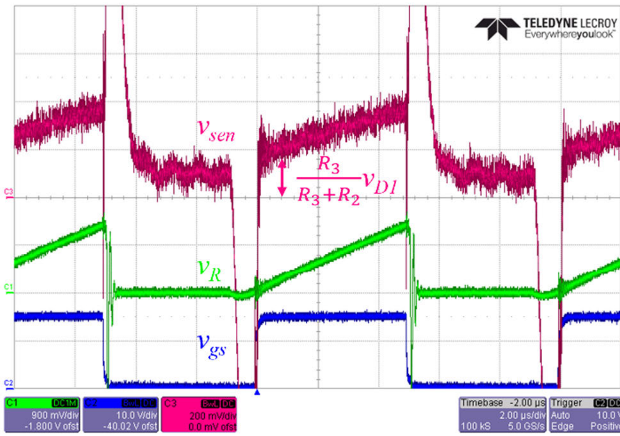

FIGURE 3. OVMC experimental waveform with a single clamp diode.

diode D_1turns on when v_{gs} is greater than v_{ds}, i.e., when the DUT is on. The voltage $v_{sen}$is given by (5) neglecting the switching noise.

$$v_{sen} = \frac{R_3}{R_3 + R_2}(v_{ds} + v_{D1}) \tag{5}$$

In (5), v_{D1} is the forward voltage drop of D_1 that makes the relationship between v_{sen} and v_{ds} nonlinear. Assuming the sensing gain of i_{ds} is unity or $i_{out} = i_{ds}$, R_{DUT} is expressed in terms of v_{sen} as in (6).

$$R_{DUT} = \frac{v_{ds}}{i_{ds}} = \frac{R_3 + R_2}{R_3}\left(\frac{v_{sen}}{i_{out}}\right) - \frac{v_{D1}}{i_{out}} \tag{6}$$

Fig. 3 shows the experimental waveform of the OVMC circuit in Fig. 2(a). Green voltage waveform v_R with 900 mV/div. scale represents the current i_{ds} measured by a 0.3-Ω shunt resistance. Magenta and blue waveforms represent v_{sen} (200 mV/div.) and v_{gs} (10 V/div.), respectively. The thick waveform of v_{sen} during the ON state of DUT indicates its low signal-to-noise ratio. Substantial distortion also occurs during the turn-off transient. The DC component of v_{sen}, $\frac{R_3}{R_3+R_2}v_{D1}$, was generated by the forward voltage drop of D_1 as explained in (5). These may result in less accurate R_{DUT} measurements, and a filter is required to attenuate these distortions. This filter complicates the design procedure and increases the circuit complexity. Even assuming v_{sen} is unaffected by the switching noise, (6) reveals that the accurate estimation of R_{DUT} is difficult by two factors, v_{D1} and i_{out}. The voltage v_{D1} varies by various factors such as the current and temperature of D_1, and utilizing its exact value is not straightforward. And division by i_{out} in (6) requires considerable resource in MCU.

Fig. 2(b) shows another OVMC with extra voltage source V_{cc} [25]. Literals v_{sen2} and V_{cc} represent the output of the OVMC and external DC voltage source, respectively. Diodes D_2 and D_3turn on when V_{cc} is greater than v_{ds}. The positive input voltage of operation amplifier (op-amp), v_+, is equal to v_{ds} plus the forward voltage drop of D_2, v_{D2}. During the on-state of the DUT, v_{sen2} is expressed as (7).

$$\begin{aligned} v_{sen2} &= v_+ + \frac{R_6}{R_5}[v_+ - (v_{ds} + v_{D2} + v_{D3})] \\ &= v_{ds} + v_{D2} - \frac{R_6}{R_5}v_{D3} \end{aligned} \tag{7}$$

In (7), v_{D3} represents the forward voltage drop of D_3, and R_5 and R_6 are resistors connected to the op-amp. The forward voltage drops cancel out each other by designing $v_{D2} = \frac{R_6}{R_5}v_{D3}$. Typically, D_1 and D_2 are similar devices and R_5 and R_6 have equal resistances. Then R_{DUT} is simply expressed as shown in (8) assuming $i_{out} = i_{ds}$.

$$R_{DUT} = \frac{v_{ds}}{i_{out}} = \frac{v_{sen2}}{i_{out}} \tag{8}$$

In practice, capacitors are added around the op-amp to form a low-pass filter and suppress the high-frequency noise in v_+. The increased components count is also a drawback of the OVMC in Fig. 2(b).

TABLE 1. Current paths, V, and R of the equivalent circuit in Fig. 3 in several PWM DC-DC converters.

Topology	Inductor current path with MOSETs ON (red) Inductor current path with MOSFETs OFF (blue)	V in Fig. 4(a)		R in Fig. 4(a)	
		MOSFETs ON	MOSFETs OFF	MOSFETs ON	MOSFETs OFF
Buck		$V_g - V_o$	$-V_o$	R_{DUT1} + R_p	R_{DUT2} + R_p
Boost		V_g	$V_g - V_o$	R_{DUT1} + R_p	R_{DUT2} + R_p
Noninverting buck-boost		V_g	$-V_o$	R_{DUT1} + R_{DUT4} + R_p	R_{DUT2} + R_{DUT3} + R_p

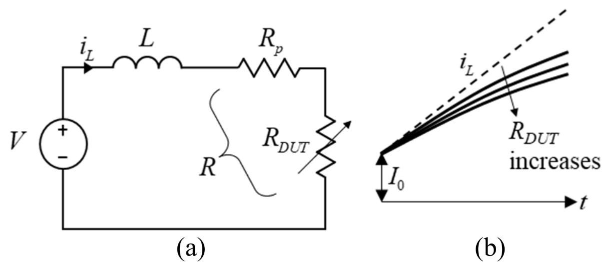

FIGURE 4. (a) Equivalent circuit of PWM converters when DUT is on. (b) Exponential waveshape of i_L by parasitic series resistances when inductor store energy.

III. PROPOSED METHOD FOR MEASURING THE INCREASE OF THE ON-STATE RESISTANCE

The RUL of a MOSFET is estimated by R_{DUT} as explained in Section II. The key idea of this paper is that the RUL estimation does not necessarily require the absolute value of R_{DUT} – only the *increment* of R_{DUT} over time suffices. The increasing trend of the resistance is estimated using Gaussian process regression, the extended Kalman filter, and the particle filter [13]. The DUT is considered expired when its R_{DUT} undergoes a 20% increase relative to its initial value [30]. The proposed method measures the increment of R_{DUT} using the inductor current information sensed by a simple circuit in pulse-width-modulated (PWM) converters.

In PWM converters, inductors store energy when its current increases, and releases the energy when the current decreases. A PWM converter when DUT is on is simplified into the equivalent circuit shown in Fig. 4(a) where i_L and V are the inductor current and equivalent voltage across the inductor. The current i_L will increase if V is positive or will decrease if V is negative. Literal L is the inductance of the inductor and R_p represents the lumped parasitic resistance in conduction path of i_L including copper trace resistance of printed circuit board, equivalent series resistance of the inductor, etc. The resistance R_p is assumed to be fixed throughout the operation, i.e., R_p is not affected by RUL. The slope of i_L is assumed constant in typical analysis of the converters as shown by the dashed line in Fig. 4(b) because R_p and R_{DUT} are assumed negligibly small. When the sum of R_p and R_{DUT}, or R, is not zero, i_L becomes exponential as expressed by the solid lines in Fig. 4(b) and (9).

$$i_L(t) = \frac{V}{R} - \left(\frac{V}{R} - I_0\right) e^{-\frac{R}{L}t} \tag{9}$$

Current I_0 in (9) and Fig. 4(b) is the initial i_L of the on-state interval. The ripple of this exponential i_L decreases as

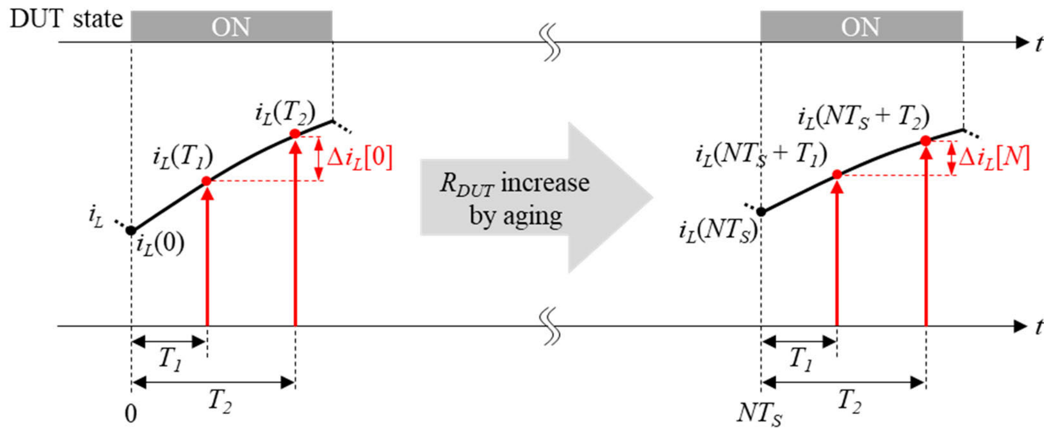

FIGURE 5. Decreasing ripple of i_L as R_{DUT} increases by the aging of DUT.

R_{DUT} increases by the aging of the DUT as depicted by the solid lines in Fig. 4(b). The proposed method measures this difference to estimate the RUL of the DUT.

Fig. 5 elaborates the measurement of the ripple of i_L. At the first turn-on interval which starts at time $t = 0$, the DUT is assumed fresh and its R_{DUT} is small. The current i_L is sampled by the MCU at two instants T_1 and T_2 as $i_L(T_1)$ and $i_L(T_2)$, respectively, while the DUT is on. Equation (10) shows $\Delta i_L[k]$ as the difference between the two sampled values in k-th switching cycle.

$$\begin{aligned}\Delta i_L[k] &= |i_L\,(kT_S + T_1) - i_L\,(kT_S + T_2)| \\ &= \left(\frac{V}{R} - i_L\,(kT_S)\right)\left|e^{-\frac{R}{L}T_1} - e^{-\frac{R}{L}T_2}\right| \end{aligned} \tag{10}$$

In (10), V and L are assumed to be constant within a switching cycle. The variation of R within a switching cycle is also assumed to be negligible although it increases due to the aging of DUT over time. The sampling time instants T_1 and T_2 are fixed throughout the operation of the converter to simplify the calculation and save resources in MCU. Fixing T_1 and T_2 also prevents other effects on the measurement such as dead time between MOSFETs. If R is numerically smaller enough than V, which is generally the case, approximation in (11) simplifies (10) into (12).

$$\frac{V}{R} \gg i_L\,(kT_S) \tag{11}$$

$$\Delta i_L\,[k] \cong \frac{V}{R}\left|e^{-\frac{R}{L}T_1} - e^{-\frac{R}{L}T_2}\right| \tag{12}$$

The difference Δi_L will decrease as R increases according to (12), or $\Delta i_L\,[0] > \Delta i_L\,[N]$ as shown in Fig. 5. The MCU can judge if the DUT is expired when Δi_L calculated by (12) becomes smaller than a certain preset value.

The proposed method has several advantages over the conventional methods. One of these advantages is that the method is more noise-robust than the conventional OVMC's explained in Section II. Literals V and i_L in (12), which should be sensed to calculate R_{DUT}, are less prone to the switching noise than the on-state voltage of the DUT such as v_{ds} in Fig. 2. These values do not need additional sensing or detection circuit because they are typically already sensed for system control purposes. The noise-robustness of the proposed method simplifies or even eliminates the low-pass filter in Fig. 2 and improves the accuracy of the estimation of the RUL.

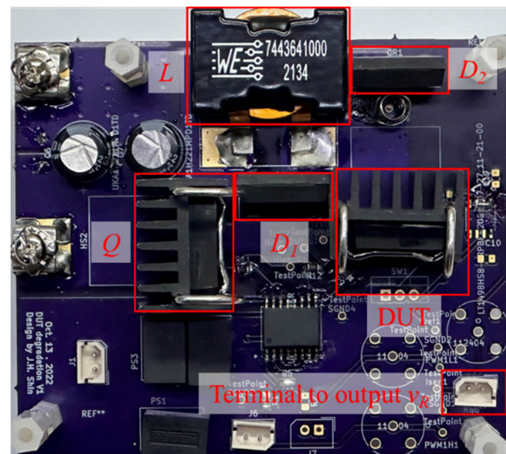

FIGURE 6. Photograph of the prototype buck-boost converter (top view).

The method is also applicable to various power conversion topologies and operation modes. Table 1 shows several DC-DC converters with inductor L. They are powered by a voltage source V_g to generate output voltage V_o. Red arrows indicate the path of i_L assuming the MOSFETs are on. The on-state V's and R's of the equivalent circuit in Fig. 4(a) and (12) for each converter are listed in Table 1.

The explanations so far have focused on the intervals in which i_L increases. It should be mentioned that the proposed method is also applicable to the intervals where i_L decreases. The on-state resistance of the devices in the freewheeling paths, indicated by the blue arrows in Table 1,

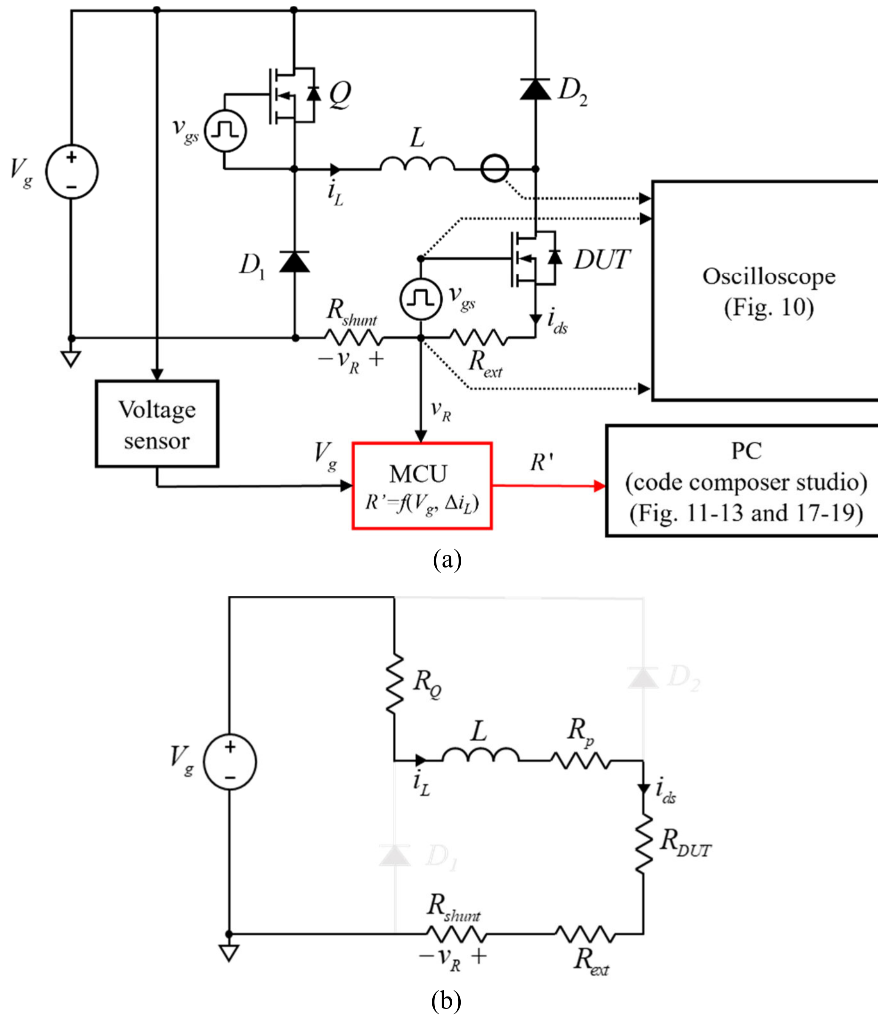

FIGURE 7. (a) Circuit diagram of the prototype buck-boost converter. (b) Equivalent circuit when *Q*and DUT are on.

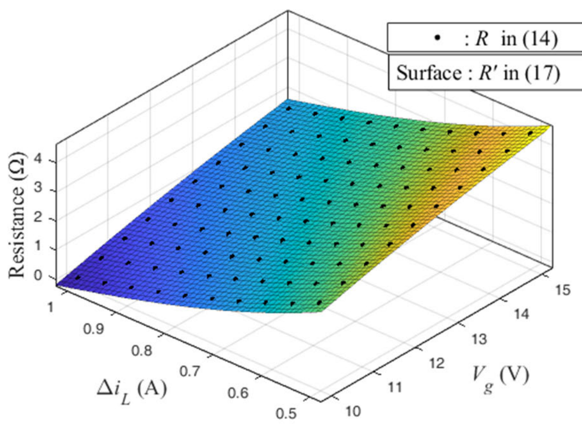

FIGURE 8. R plotted as function of V_g and $\Delta\, i_L$.

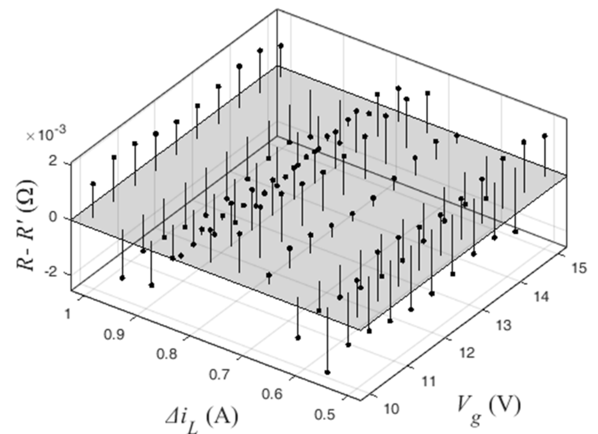

FIGURE 9. Resistance error as function of V_g and Δi_L.

can also be measured. Equations (9), (10), and (12) and inequality (11) hold the same in these cases except that V is negative.

The proposed method also works in the PWM converters operating in discontinuous conduction mode. The current i_L is zero at the beginning of each switching cycle,

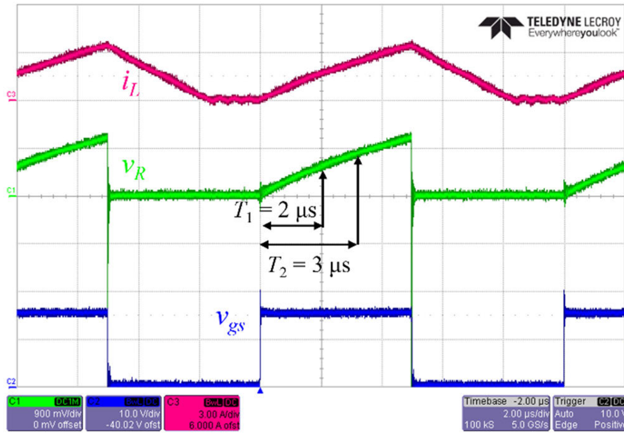

FIGURE 10. Experimental waveforms.

i.e., $i_L(kT_S) = 0$. The semi-equal sign in (12) is replaced by an equal sign in this case.

IV. EXPERIMENTS

A. HARDWARE SETUP

The experiments verify the proposed method in a non-inverting buck-boost converter of which input and output are the same. Figs. 6 and 7(a) show the photograph of the prototype converter and the experimental setup around it, respectively. In Fig. 7(a), V_g is the input voltage, and v_{gs} is the gate signal for both MOSFETs Q and DUT. Resistor R_{ext} is an external resistor to emulate the aging or temperature-dependent resistance change of DUT: zero R_{ext} simulates fresh DUT; non-zero R_{ext} simulates aged DUT or DUT operating in high temperature. Diodes D_1 and D_2 are the freewheeling diodes. Resistor R_{shunt} is a shunt resistor for current sensing: Setting the negative terminal of V_g as ground, v_R represents the voltage across R_{shunt} and satisfies (13).

$$v_R = R_{shunt} \cdot i_{ds} \tag{13}$$

For higher efficiency, a non-contact current sensor such as a Rogowski coil [31] or Hall sensor can replace R_{shunt}. This current sensor should be designed or chosen carefully since its bandwidth may distort the sampled i_L and lowers the accuracy of measuring the on-state resistance. To avoid this distortion, bandwidth as high as 9 times the switching frequency of PCS is recommended. Explanations on the sensor bandwidth is provided in Appendix.

In Fig. 7(a), the MCU, depicted within the red box, senses V_g and $v_R$without noise sensitive v_{ds}, computes the function $f(V_g, \Delta i_L)$, and transmits R' to personal computer, PC. A detailed explanation of how to find $f(V_g, \Delta i_L)$ is presented in the next section.

The equivalent circuit when Q and DUT are ON is illustrated in Fig. 7(b), which is similar to Fig. 4(a). Currents i_L and i_{ds} are the same in Fig. 7(b). Substituting (13) into (12) and replacing V into V_g yields (14), where the total resistance

TABLE 2. Parameters of experiment circuit.

Parameter	Description
V_g	10 V
L	10 μH
Q and DUT	STW58N60DM2AG, FQA28N15, C3M0120090D, or IMW120R350M1H
Switching frequency	100 kHz
D_1 and D_2	APT30S20BG
R_{shunt}	0.3 Ω
R_{ext} (emulating fresh DUT)	0 Ω
R_{ext} (emulating aged DUT)	15 mΩ, 18.75 mΩ, and 25 mΩ
T_1	2 μs
T_2	3 μs
MCU	TMS320F280049C

R is defined in (15).

$$\Delta i_L[k] = \frac{|v_R(kT_S + T_1) - v_R(kT_S + T_2)|}{R_{shunt}} \cong \frac{V_g}{R}\left|e^{-\frac{R}{L}T_1} - e^{-\frac{R}{L}T_2}\right| \tag{14}$$

$$R = \left(R_{DUT} + \frac{R_{ext}}{2}\right) + \left(R_Q + \frac{R_{ext}}{2}\right) + R_{shunt} + R_p \tag{15}$$

Equation (15) assumes that Q and DUT age at the same rate, and thus the addition of R_{ext} indicates that resistance increase in DUT is equal to $R_{ext}/2$.

The proposed method verifies that v_R in (13) decreases as R in (15) increases by inserting R_{ext}. Also, various MOSFETs are utilized as Q and DUT to further verify the feasibility of the proposed method. The MOSFETs used in the experiment are STW58N60DM2AG, FQA28N15, C3M120090D, and IMW120R350M1H, of which on-state resistances are 52 mΩ, 67 mΩ, 120 mΩ, and 350 mΩ, respectively [32], [33], [34], [35]. The specifications of the circuit components are shown in Table 2.

B. SOFTWARE SETUP

Assuming T_1, T_2, and L are fixed, R depends on $\Delta i_L[k]$ and V_g in (14). Calculating R using (14) contains exponential and logarithmic operations which require considerable resource of the MCU. For simpler and quicker calculation, curve fitting technique is used to express R as a polynomial of two variables, $\Delta i_L[k]$ and V_g.

The range of V_g is set to the operating window for PCS and the boundary of Δi_L is defined as the value that can be varied by V_g. The maximum Δi_L is expressed as in (16).

$$\Delta i_{L_max} = (T_2 - T_1)\frac{V_{g_min}}{L} \tag{16}$$

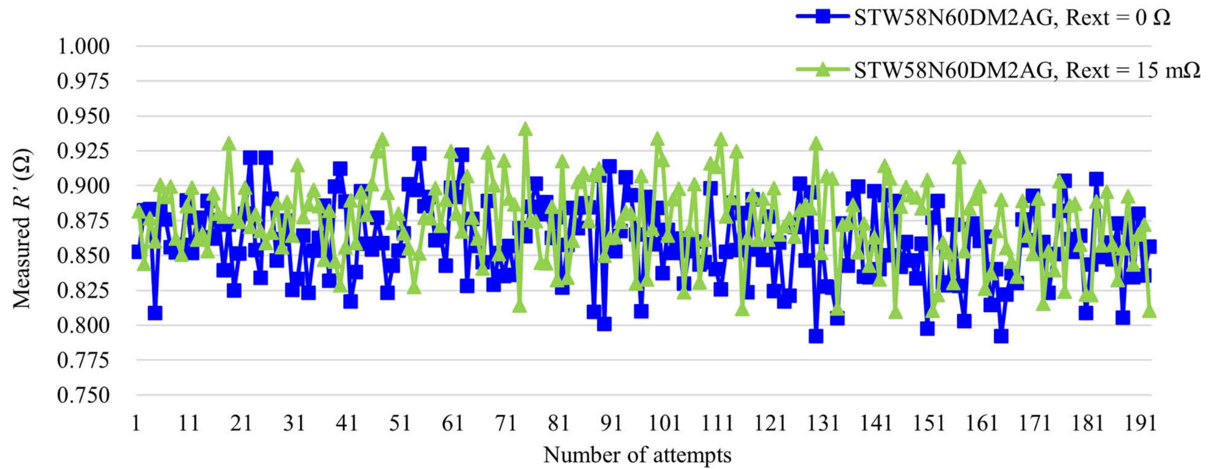

FIGURE 11. Experimental results when the DUT is STW58N60DM2AG and R_{ext} = 0 or 15 m Ω.

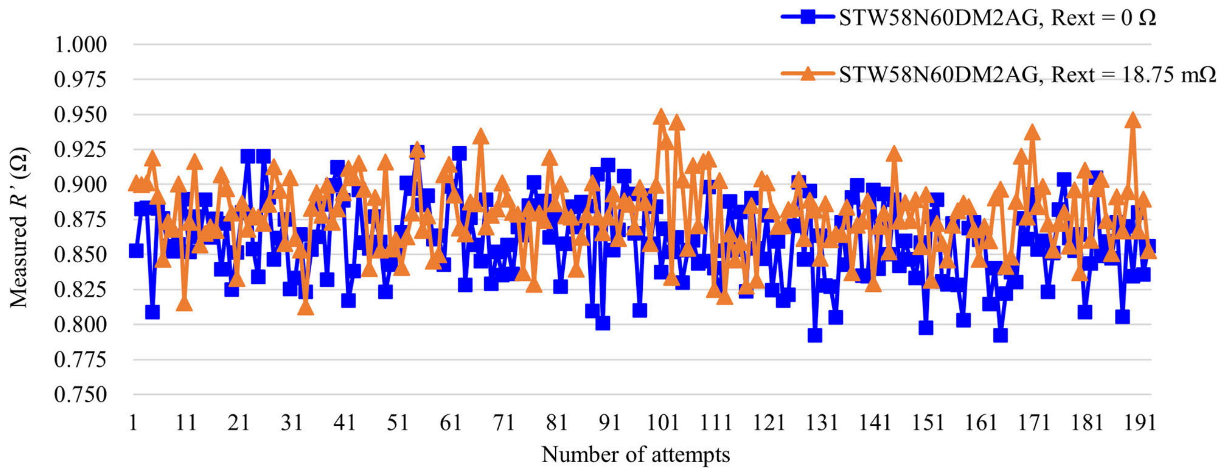

FIGURE 12. Experimental results when the DUT is STW58N60DM2AG and Rext = 0 or 18.75 m Ω.

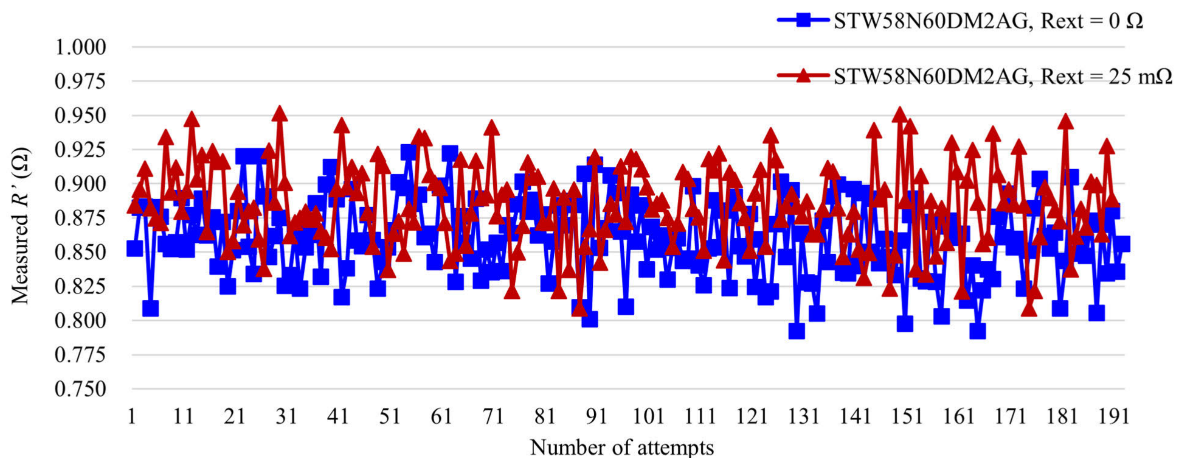

FIGURE 13. Experimental results when the DUT is STW58N60DM2AG and R_{ext} = 0 or 25 mΩ.

In (16), $V_{g_\min}$ represents minimum of $V_g$and Δi_{L_max} means maximum Δi_L that corresponds to zero R in (14) when V_g in Fig. 7(a) is $V_{g_\min}$. If $\Delta i_L > \Delta i_{L_max}$ and $V_g = V_{g_min}$, R becomes negative or imaginary in (14), which has little

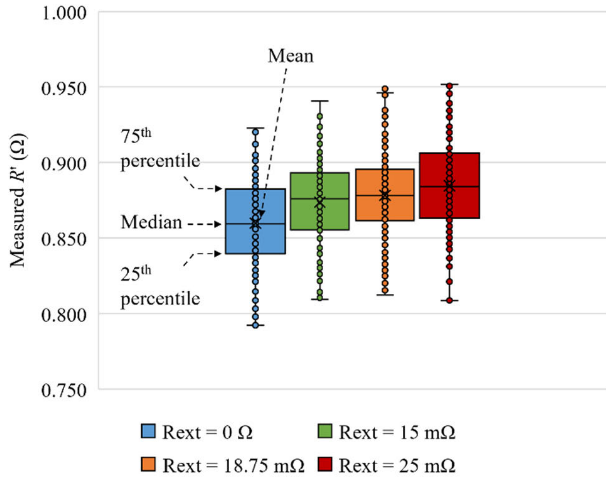

FIGURE 14. Boxplot of R' when R_{ext} = 0, 15, 18.75, or 25 mΩ.

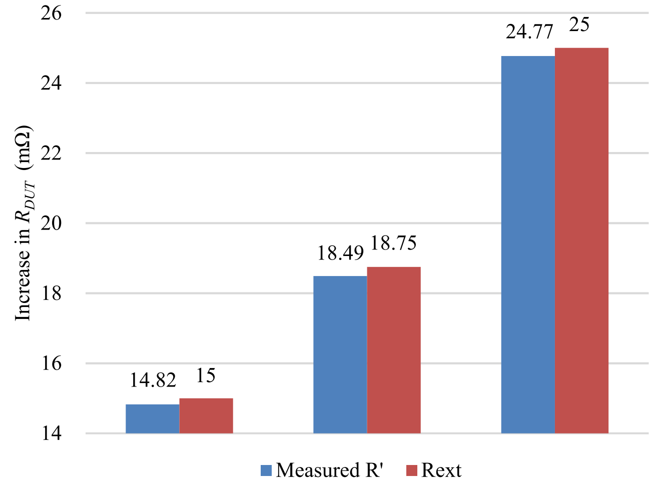

FIGURE 16. Comparison of the difference between measured R' and R_{ext}.

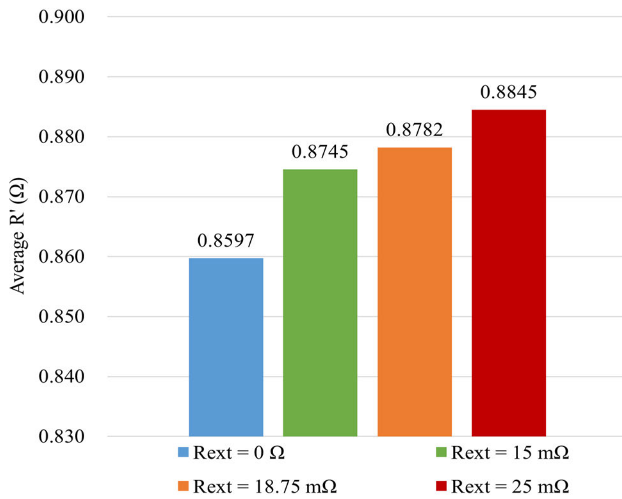

FIGURE 15. Average R' of experimental results shown in Figs. 11-14.

meaning. Black dots in Fig. 8 are the calculated R using (14) by sweeping V_g from 10 to 15 V and Δi_L 0.5 to 1 A. Setting the approximated R or R' is a third-order function of Δi_L and V_g as in (17), the surface in Fig. 8 represents R'.

$$\begin{aligned} R' = f\left(V_g, \Delta i_L\right) &= p_{00} + p_{10}V_g + p_{01}\Delta i_L \\ &+ p_{20}V_g^2 + p_{11}V_g\Delta i_L + p_{02}\Delta i_L^2 \\ &+ p_{30}V_g^3 + p_{21}V_g^2\Delta i_L + p_{12}V_g\Delta i_L^2 + p_{03}\Delta i_L^3 \end{aligned} \tag{17}$$

In (17), p_{ij} ($i = 0, 1, 2,$ or 3; $j = 0, 1, 2,$ or 3) is a coefficient of the term $V_g^i \Delta i_L^j$ which were generated by the multivariate polynomial function of MATLAB curve-fitting tool [36]. The curve-fitting tool calculates p_{ij} by fitting (17) to the black dots in Fig. 8 using the least-squares method. The fitted p_{ij}'s are in Table 3. The error $R - R'$ is plotted in Fig. 9. It is verified that the error between R calculated by (14) and R' calculated by (17) is less than 2 mΩ of which effect on sensing the increase of R_{DUT} is negligible. Equation (17) is used as $f(V_g, \Delta i_L)$, shown in Fig. 7(a). Using the higher order terms of Δi_L and V_g. yields the smaller $R - R'$ in Fig. 9, while it requires more computational resource of MCU as a trade-off.

The analog-to-digital converters (ADCs) in the MCU convert $i_L(T_1)$ and $i_L(T_2)$ into digital bits. Variables ADC_VRT1, ADC_VRT2, and ADC_DelI in the MCU contain the data converted from $v_R(kT_S + T_1)$, and $v_R(kT_S + T_2)$, and $\Delta i_L[k]$, respectively. Sensing gain is decided as $2^{12}/3.3 = 1241$ since the ADCs are 12 bits and powered by 3.3-V voltage source. Equation (18) shows the relationship between the physical quantities and variables in the MCU.

$$\text{ADC_VRT1} = 1241 \cdot v_R\left(kT_S + T_1\right) \tag{18a}$$

$$\text{ADC_VRT2} = 1241 \cdot v_R\left(kT_S + T_2\right) \tag{18b}$$

$$\begin{aligned} \text{ADC_DelI} &= 1241 \cdot \Delta i_L\left[k\right] \\ &= \left(\frac{\text{ADC_VRT2} - \text{ADC_VRT1}}{R_{shunt}}\right) \end{aligned} \tag{18c}$$

A portion of the C code programmed in the MCU to realize the proposed method is shown in Table 4. Literal V_{g_gain} in Table 4 is a parameter to compensate the gain of the voltage sensor shown in Fig. 7(a). Division by 1241 was rephased by multiplying 0.0008058 to reduce computation time in MCU. The proposed method calculates R' through the ADC interrupt service routine (ISR) in the MCU, and the time taken by the ISR was less than 2 μs. This means that the time taken to calculate R' is less than 2 μs.

C. RESULTS AND DISCUSSION

The proposed method is verified by comparing the calculated R' by the MCU with zero, 15-mΩ, 18.75-mΩ, or 25-mΩ R_{ext}. Fig. 10 illustrates the experimental waveforms. Magenta, blue, and green waveforms represent i_L (3 A/div.), v_{gs} (10 V/div.), and v_R(900 mV/div.), respectively. In Fig. 10, i_L at the top was measured by a 50-MHz bandwidth current probe CP030 manufactured by LeCroy [37]. The waveform is free of noise compared to the waveform of v_{sen} in Fig. 3. As indicated in the v_R waveform in Fig. 10, the MCU measures v_R twice, i.e., the ADCs converts v_R at the instant 2 μs and 3 μs

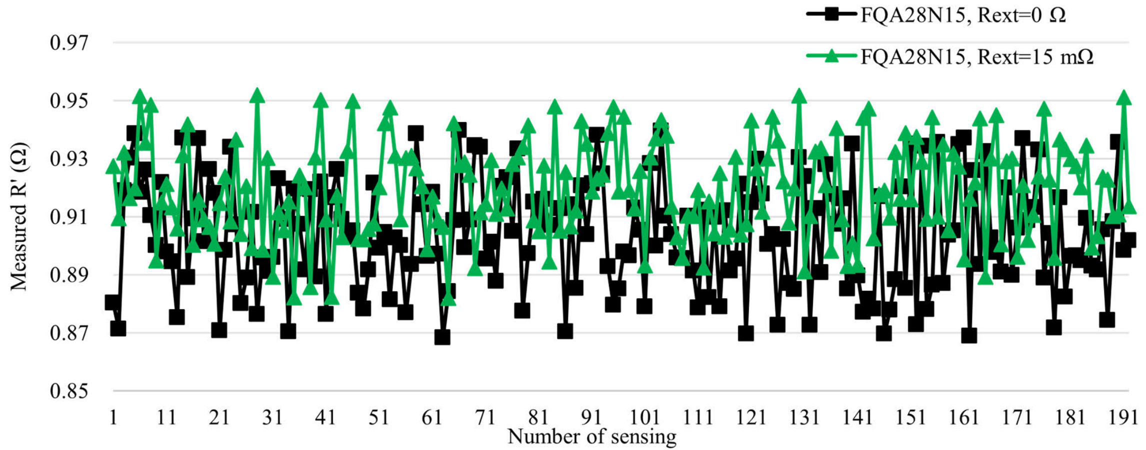

FIGURE 17. Experimental results when the DUT is FQA28N15 and $R_{ext} = 0$ or 25 m Ω.

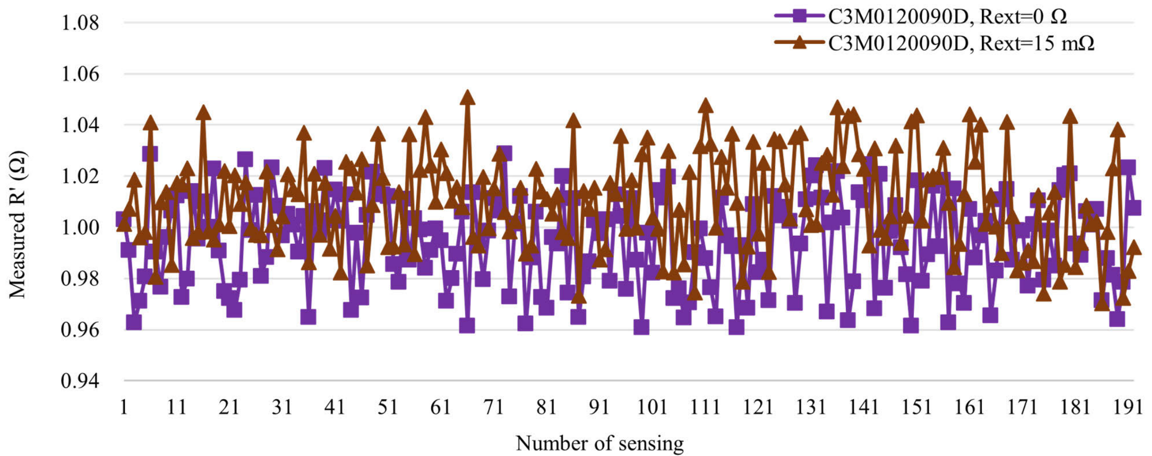

FIGURE 18. Experimental results when the DUT is C3M120090D and $R_{ext} = 0$ or 25 m Ω.

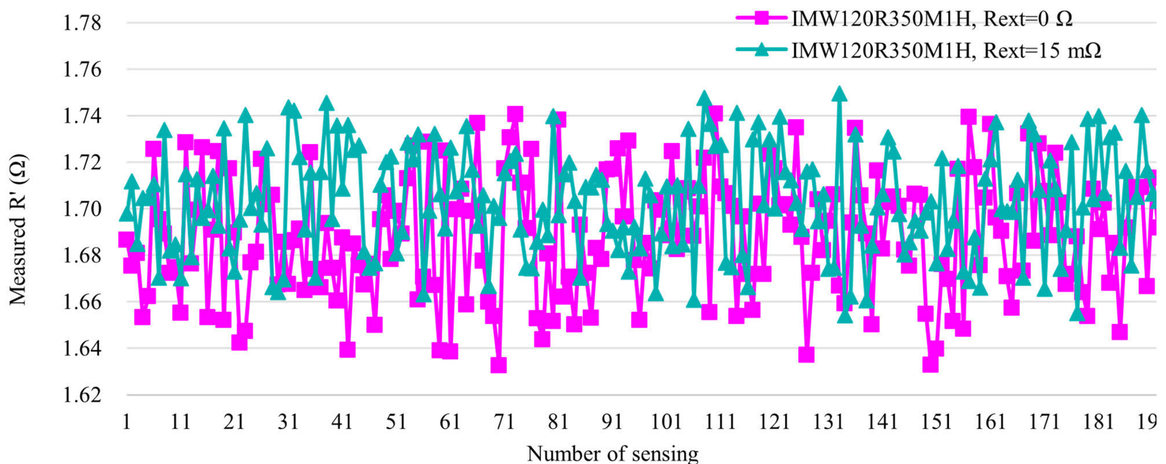

FIGURE 19. Experimental results when the DUT is IMW120R350M1H and $R_{ext} = 0$ or 25 mΩ.

after the rise of v_{gs}. No ringing or oscillation in v_R at these instants proves the noise-robustness of the proposed method.

Figs. 11, 12, and 13 illustrate R' calculated by the code shown in Table 4 programmed in the MCU when the DUT

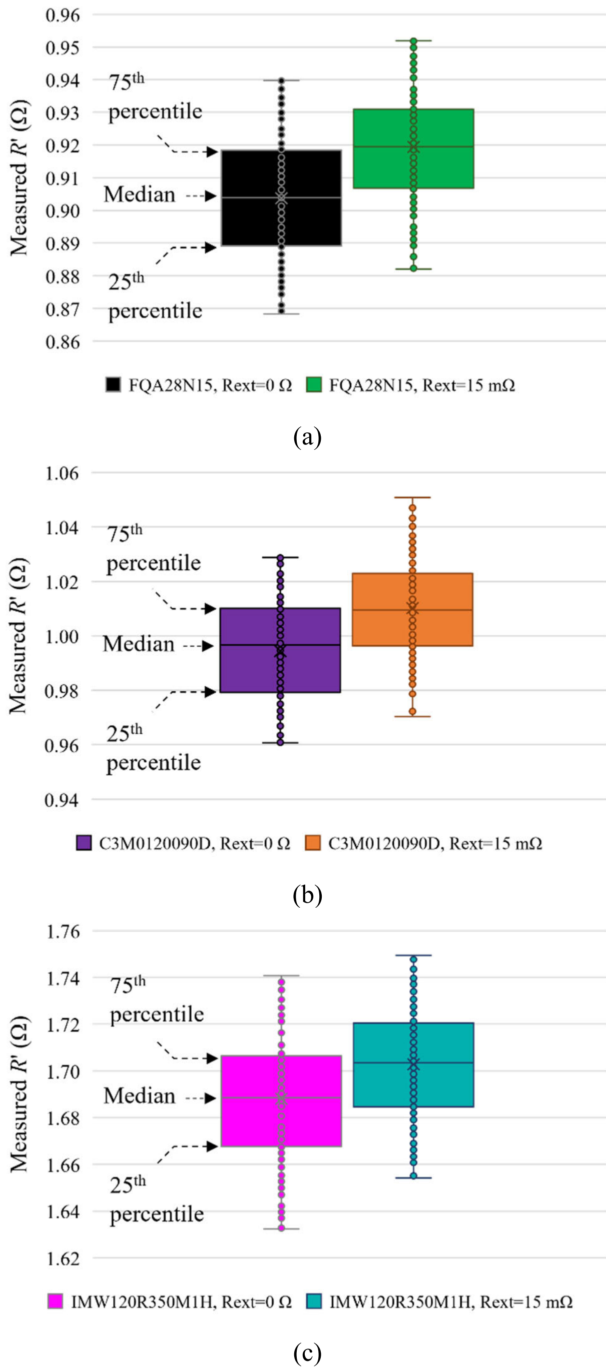

FIGURE 20. Boxplot of R' when $R_{ext} = 0$ or 15 mΩ and DUT is (a) FQA28N15, (b) C3M0120090D, or (c) IMW120R350M1H.

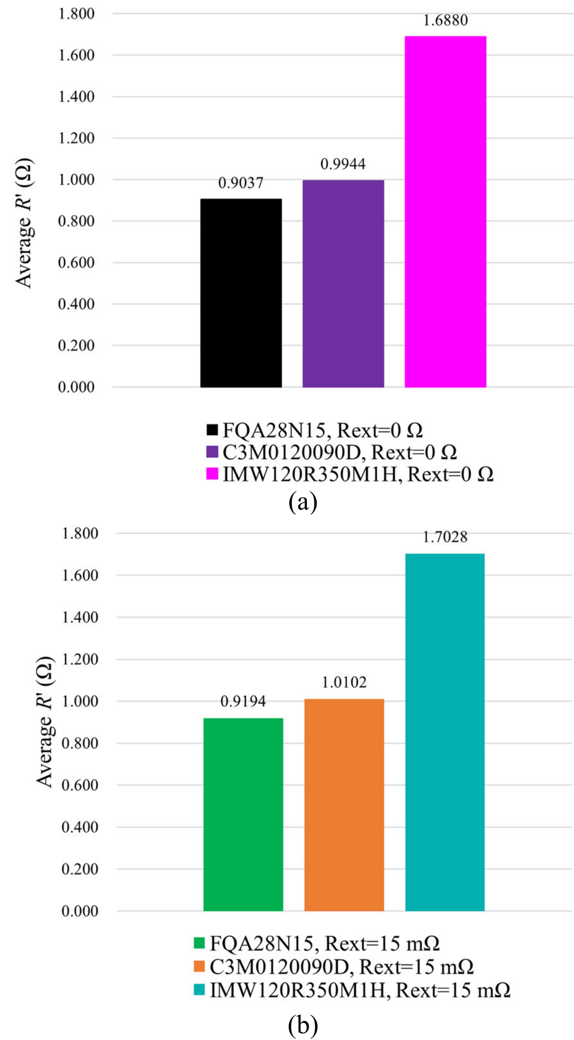

FIGURE 21. Average R' of experimental results shown in Figs. 17-19 when R_{ext} = (a) 0 or (b) 15 mΩ.

is STW58N60DM2AG. The x-axis represents the number of sensing v_R. The values of R'were monitored online, or while the circuit in Fig. 7(a) is operating, by utilizing Texas Instruments' code composer studio. Green markers in Fig. 11, orange in Fig. 12, and red in Fig. 13 represent the measured R' when R_{ext} = 15, 18.75, or 25 mΩ, respectively. Blue markers in Figs. 11, 12, and 13 are when $R_{ext} = 0$. Fig. 14 shows a boxplot of R' when R_{ext} = 0, 15 mΩ, 18.75 mΩ, or 25 mΩ, demonstrating that the measured R' increases as R_{ext} increases. Fig. 15 compares the average R's shown in the boxplot in Fig. 14 which are 0.8597 Ω, 0.8745 Ω, 0.8782 Ω, and 0.8845 Ω when R_{ext} = 0, 15 mΩ, 18.75 mΩ, and 25 mΩ, respectively. Fig. 16 shows the increments of R' and R_{ext} were highly similar to each other though the absolute values of R' and R_{ext} were not same to each other. The 14.8-mΩ, 18.49-mΩ, and 24.8-mΩ increase in R' corresponds to 15-mΩ, 18.75-mΩ, and 25-mΩ increase in R_{ext}, respectively. The accuracy of measuring the increase of the on-state resistance is therefore 98.6%, 98.6%, and 99.2%.

MOSFETs Q and DUT in Fig. 7(a) are varied to further verify the effectiveness of the proposed method. Figs. 17, 18, and 19 show calculated R' by MCU when Q and the DUT is FQA28N15, C3M120090D, and IMW120R350M1H, respectively. Black markers in Fig. 17, purple in Fig. 18, and pink in Fig. 19 represent the measured R' when $R_{ext} = 0$. Green markers in Fig. 17, brown in Fig. 18, and cyan in Fig. 19 represent the measured R' when R_{ext} = 15 mΩ.

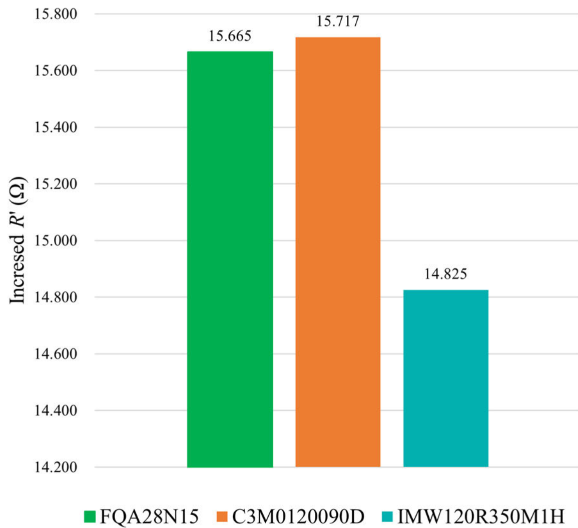

FIGURE 22. Increased resistance when adding an extra series-connected 15-mΩ resistor for each device.

TABLE 3. Coefficients of fitted function.

Parameter	Description
p_{00}	2.211
p_{10}	0.9838
p_{01}	-16.94
p_{20}	-0.03922
p_{11}	-0.01832
p_{02}	11.79
P_{30}	0.0006949
p_{21}	0.0002357
p_{12}	0.004273
p_{03}	-3.552

TABLE 4. C code to realize the proposed method.

Function	C Code
$\Delta i_L[k]$	ADC_DelI = abs(ADC_VRT2 – ADC_VRT1)*(1/R_{shunt}); DelI=ADC_DelI*(1/1241);
V_g	V_g = ADC_Vg*V_{g_gain}*0.0008058;
R	R = p00+p10*V_g +p01*DelI+p20*V_g*V_g +p11*V_g*DelI+p02*DelI*DelI +p30*V_g*V_g*V_g+p21*V_g*V_g*DelI +p12*V_g*DelI*DelI +p03*DelI*DelI*DelI;

Figs 17, 18, and 19 demonstrate that R' increases as R_{ext} increases, and for a more visual representation, R' data is depicted as a boxplot in Fig. 20. The boxplot shows that there is a noticeable increase in R' when $R_{ext} = 15$ mΩ. Fig. 21 shows the average values of Figs. 17, 18, and 19, where Fig. 21(a) and Fig. 21(b) are for $R_{ext} = 0$ or 15 mΩ, respectively. In Fig. 21(a), the average R' values are 0.9037 Ω, 0.9944 Ω, and 1.688 Ω when the DUT is FQA28N15, C3M120090D, or IMW120R350M1H, respectively. The corresponding average R' values are 0.9194 Ω, 1.0102 Ω, and 1.7028 Ω in Fig. 21(b). Fig. 22 shows the difference in average R' before and after the addition of R_{ext}. The increased R' values when DUT is FQA28N15, C3M120090D, or IMW120R350M1H are determined 15.66 mΩ, 15.71 mΩ, and 14.82 mΩ, respectively, with accuracies of 95.8%, 95.5%, and 98.8%, respectively.

V. CONCLUSION

A method for online measuring on-state resistance to estimate the RUL of a power semiconductor device has been proposed. The proposed method does not measure the noisy on-state voltage of power semiconductor device like conventional OVMCs, which increases the accuracy of the measurement and simplifies the sensing circuit. The proposed method accurately measures the increase of R_{DUT} by sensing noise-robust quantities such as inductor current and DC voltage. The proposed method also requires no additional filters and arithmetic circuits for simple implementation.

Motivated by the fact that the increased R_{DUT} by aging also increases the equivalent resistance of the PWM converter while DUT is ON, the converter is modeled into the equivalent resistance-inductance (RL) circuit with a series-connected voltage source. The proposed method samples the inductor current twice in a single switching period, and the difference between the two sampled values are utilized to estimate the equivalent resistance of the RL circuit. A third-order polynomial was derived by curve fitting the simulated resistances for various inductor current differences and voltages. The proposed method allows the MCU to calculate the increased resistance, which in turn allows the MCU to determine the expiration of the MOSFET on its own.

The concept of the proposed online on-state resistance measurement was applied to the prototype non-inverting buck-boost converter. The increase of the on-state resistance of a MOSFET by aging in the prototype converter was emulated by an extra series-connected 15-mΩ, 18.75-mΩ, or 25-mΩ resistor. The resistance increase by these resistors were measured 14.8 mΩ (98.6% accuracy), 18.49 mΩ (98.6% accuracy), and 24.8 mΩ (99.2% accuracy), respectively.

The proposed method was verified on various MOSFETs. Various MOSFETs were applied to the prototype converter to observe the increase in resistance before and after an extra series-connected 15-mΩ resistor was attached. The resistance increased by 15-mΩ resistor was obtained 15.66 mΩ (95.8% accuracy), 15.71 mΩ (95.5% accuracy), and 14.82 mΩ (98.8% accuracy) when DUT is FQA28N15, C3M120090D, and IMW120R350M1H, respectively. The proposed method showed at least 95.5% accurate on a variety of MOSFETs. The MOSFET was judged to be expired if the resistance

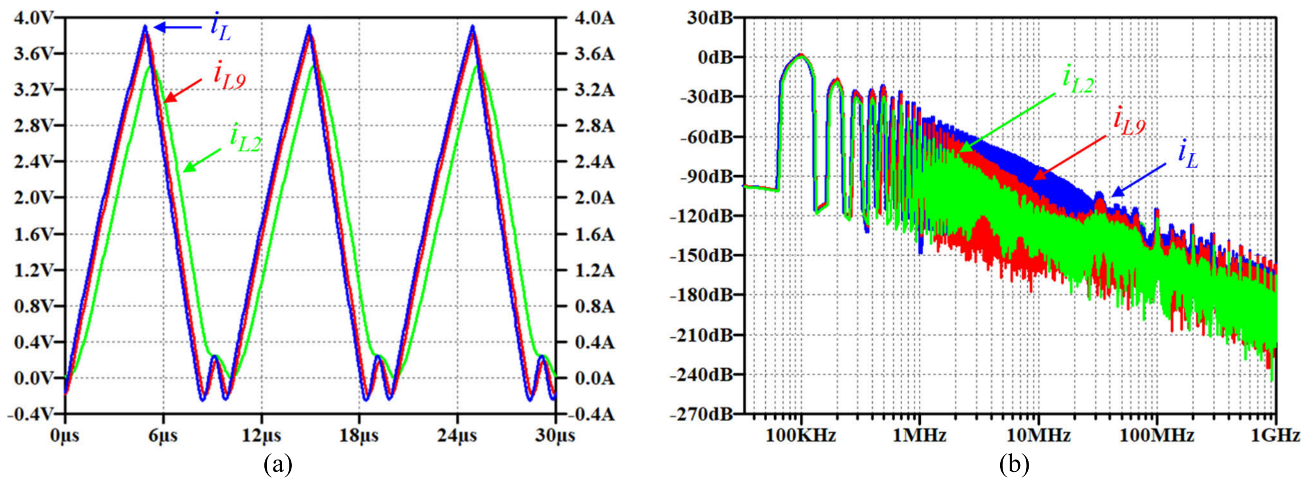

FIGURE 23. (a) Original and sensed i_L waveforms and (b) their FFT results.

increase measured by the proposed method is higher than 20% of the initial on-state resistance of MOSFET. This proves the feasibility of the proposed method to estimate the RUL of the MOSFETs.

APPENDIX

If a current sensor is utilized instead of R_{shunt} in Fig. 7, its bandwidth should be higher than 9 times the switching frequency. Fourier series expression of i_L is in (19).

$$i_L(t) = a_0 + \sum_{n=1}^{\infty} \left(a_n \sin(2\pi f_0 nt) + b_n \cos(2\pi f_0 nt)\right) \quad (19)$$

In (19), a_0 and f_0 are the DC component and fundamental frequency of i_L. Coefficients a_n and b_n represent the Fourier coefficients of the n-th harmonic. In Fig. 23(a), blue waveform is the original waveform of i_L. Green waveform i_{L2} and red waveform i_{L9} depict the sensed i_L when its bandwidth is set to twice and nine times f_0, respectively. The wider bandwidth guarantees the less distortion and delay in the sensed i_L. Fig. 23(b) shows the fast Fourier transform of the waveforms in Fig. 23(a). The green waveform with the twice $f_0$bandwidth shows more distortion in the high frequency region than the red waveform with nine times f_0 bandwidth. These distortions can increase the error between the original and sensed i_L and lowers the accuracy of estimating RUL.

REFERENCES

[1] S. Yang, A. Bryant, P. Mawby, D. Xiang, L. Ran, and P. Tavner, ''An industry-based survey of reliability in power electronic converters,'' *IEEE Trans. Ind. Appl.*, vol. 47, no. 3, pp. 1441–1451, May 2011.

[2] A. Abuelnaga, M. Narimani, and A. S. Bahman, ''Power electronic converter reliability and prognosis review focusing on power switch module failures,'' *J. Power Electron.*, vol. 21, no. 6, pp. 865–880, Jun. 2021.

[3] J.-H. Hwang, L. M. Halabi, Y. Ko, and K.-B. Lee, ''Lifetime-based fault tolerant strategy for three-level hybrid ANPC inverters,'' *J. Power Electron.*, vol. 23, no. 2, pp. 363–373, Feb. 2023.

[4] A. Ginart, M. J. Roemer, P. W. Kalgren, and K. Goebel, ''Modeling aging effects of IGBTs in power drives by ringing characterization,'' in *Proc. Int. Conf. Prognostics Health Manage.* Denver, CO, USA, Oct. 2008, pp. 1–7.

[5] M. A. Rodriguez, A. Claudio, D. Theilliol, and L. G. Vela, ''A new fault detection technique for IGBT based on gate voltage monitoring,'' in *Proc. IEEE Power Electron. Spec. Conf.*, Jun. 2007, pp. 1001–1005.

[6] J. Shin and J. Shin, ''Testbed of power MOSFET aging including the measurement of on-state resistance,'' *Trans. Korean Inst. Power Electron.*, vol. 27, no. 3, pp. 206–213, Jun. 2022.

[7] S. Baba, A. Gieraltowski, M. Jasinski, F. Blaabjerg, A. S. Bahman, and M. Zelechowski, ''Active power cycling test bench for SiC power MOSFETs—Principles, design, and implementation,'' *IEEE Trans. Power Electron.*, vol. 36, no. 3, pp. 2661–2675, Mar. 2021.

[8] O. Alatise, I. Kennedy, G. Petkos, and A. Koh, ''Reliability of repetitively avalanched wire-bonded low-voltage discrete power trench n-MOSFETs,'' *IEEE Trans. Device Mater. Rel.*, vol. 11, no. 1, pp. 157–163, Mar. 2011.

[9] U.-M. Choi, F. Blaabjerg, S. Jørgensen, S. Munk-Nielsen, and B. Rannestad, ''Reliability improvement of power converters by means of condition monitoring of IGBT modules,'' *IEEE Trans. Power Electron.*, vol. 32, no. 10, pp. 7990–7997, Oct. 2017.

[10] U.-M. Choi and F. Blaabjerg, ''Separation of wear-out failure modes of IGBT modules in grid-connected inverter systems,'' *IEEE Trans. Power Electron.*, vol. 33, no. 7, pp. 6217–6223, Jul. 2018.

[11] U.-M. Choi, F. Blaabjerg, and S. Jørgensen, ''Power cycling test methods for reliability assessment of power device modules in respect to temperature stress,'' *IEEE Trans. Power Electron.*, vol. 33, no. 3, pp. 2531–2551, Mar. 2018.

[12] U.-M. Choi, F. Blaabjerg, and S. Jørgensen, ''Study on effect of junction temperature swing duration on lifetime of transfer molded power IGBT modules,'' *IEEE Trans. Power Electron.*, vol. 32, no. 8, pp. 6434–6443, Aug. 2017.

[13] J. R. Celaya, A. Saxena, S. Saha, and K. Goebel, ''Prognostics of power MOSFETs under thermal stress accelerated aging using data-driven and model-based methodologies,'' in *Proc. Annu. Conf. PHM Soc.*, 2011, vol. 3, no. 1. [Online]. Available: https://papers.phmsociety.org/index.php/phmconf/article/view/1995

[14] J. Celaya, A. Saxena, P. Wysocki, S. Saha, and K. Goebel, ''Towards prognostics of power MOSFETs: Accelerated aging and precursors of failure,'' in *Proc. Annu. Conf. PHM Soc.*, 2010, vol. 2, no. 1. [Online]. Available: https://www.papers.phmsociety.org/index.php/phmconf/article/view/1761

[15] Y. Peng, S. Zhao, and H. Wang, ''A digital twin based estimation method for health indicators of DC–DC converters,'' *IEEE Trans. Power Electron.*, vol. 36, no. 2, pp. 2105–2118, Feb. 2021.

[16] U.-M. Choi and F. Blaabjerg, ''Real-time condition monitoring of IGBT modules in PV inverter systems,'' in *Proc. 10th Int. Conf. Integr. Power Electron. Syst.*, Stuttgart, Germany, Mar. 2018, pp. 1–5.

[17] B. Kohlhepp, D. Kübrich, M. Tannhäuser, A. Hoffmann, and T. Dürbaum, ''Test setup for dynamic ON-state resistance measurement of high- and low-voltage GaN-HEMTs under hard and soft switching operations,'' *IEEE Trans. Instrum. Meas.*, vol. 69, no. 10, pp. 7740–7751, Oct. 2020.

[18] F. Yang, C. Xu, E. Ugur, S. Pu, and B. Akin, "Design of a fast dynamic on-resistance measurement circuit for GaN power HEMTs," in *Proc. IEEE Transp. Electrific. Conf. Expo (ITEC)*, Long Beach, CA, USA, Jun. 2018, pp. 359–365.

[19] *Current Sensing Single Channel Driver, IR2127(s)/IR2128(s)/IR21271 (S)&(PbF) Datasheet*, Infineon, Neubiberg, Germany, Aug. 2009.

[20] R. Li, X. Wu, S. Yang, and K. Sheng, "Dynamic on-state resistance test and evaluation of GaN power devices under hard- and soft-switching conditions by double and multiple pulses," *IEEE Trans. Power Electron.*, vol. 34, no. 2, pp. 1044–1053, Feb. 2019.

[21] G. Zulauf, M. Guacci, J. M. Rivas-Davila, and J. W. Kolar, "The impact of multi-MHz switching frequencies on dynamic on-resistance in GaN-on-Si HEMTs," *IEEE Open J. Power Electron.*, vol. 1, pp. 210–215, 2020.

[22] U.-M. Choi, S. Jørgensen, and F. Blaabjerg, "Advanced accelerated power cycling test for reliability investigation of power device modules," *IEEE Trans. Power Electron.*, vol. 31, no. 12, pp. 8371–8386, Dec. 2016.

[23] S. Dusmez and B. Akin, "An accelerated thermal aging platform to monitor fault precursor on-state resistance," in *Proc. IEEE Int. Electr. Mach. Drives Conf. (IEMDC)*, Coeur d'Alene, ID, USA, May 2015, pp. 1352–1358.

[24] S. Beczkowski, P. Ghimre, A. R. de Vega, S. Munk-Nielsen, B. Rannestad, and P. Thøgersen, "Online V_{ce} measurement method for wear-out monitoring of high power IGBT modules," in *Proc. 15th Eur. Conf. Power Electron. Appl. (EPE)*, Lille, France, Sep. 2013, pp. 1–7.

[25] M. Guacci, D. Bortis, and J. W. Kolar, "On-state voltage measurement of fast switching power semiconductors," *CPSS Trans. Power Electron. Appl.*, vol. 3, no. 2, pp. 163–176, Jun. 2018.

[26] B. Yu, L. Wang, and D. Ahmed, "Drain–source voltage clamp circuit for online accurate ON-state resistance measurement of SiC MOSFETs in DC solid-state power controller," *IEEE J. Emerg. Sel. Topics Power Electron.*, vol. 8, no. 1, pp. 331–342, Mar. 2020.

[27] J. Shin and J. Shin, "Device and method for diagnosing aging state of power semiconductor based on non-contact," Korea Patent App. 10-2022-0 063 983, May 2022.

[28] *Isolated Compact IGBT Gate Driver With Current Sense, NCD57085, NCV57085 Datasheet*, Onsemi, Phoenix, AZ, USA, Mar. 2021, p. 3.

[29] J. Shin, "Apparatus for diagnosing the aging state of power semiconductor and method thereof," Korea Patent App. 10-2022-0 016 744, Feb. 2022.

[30] J. Lutz, H. Schlangenotto, U. Scheuermann, and R. D. Doncker, *Semiconductor Power Device-Physics, Characteristic, Reliability*. New York, NY, USA: Springer-Verlag, 2011, ch. 1.

[31] S. Ziegler, R. C. Woodward, H. Ho-Ching Iu, and L. J. Borle, "Current sensing techniques: A review," *IEEE Sensors J.*, vol. 9, no. 4, pp. 354–376, Apr. 2009.

[32] *MDmesh™ DM2 Power MOSFET in a TO-247 Package*, document STW58N60DM2AG, STMicroelectronics, Geneva, Switzerland, Jul. 2015.

[33] *N-Channel QFET® MOSFET*, document FQA28N15, FAIRCHILD, 2014.

[34] *Silicon Carbide Power MOSFET C3MTM MOSFET Technology*, document C3M0120090D, CREE, 2020.

[35] *CoolSiC™ 1200V SiC Trench MOSFET Silicon Carbide MOSFET*, document IMW120R350M1H, Infineon, 2020.

[36] *Curve Fitting Toolbox User's Guide, Version 3.5.12*, MathWorks, Inc., Natick, MA, USA, 2020.

[37] *CP030 Current Probe*, Teledyne Lecroy, Chestnut Ridge, NY, USA, Jan. 2013.

JUNHO SHIN received the B.S. degree in energy system engineering from Chung-Ang University, Seoul, South Korea, in 2022, where he is currently pursuing the M.S. degree with the Department of Smart Cities.

His research interests include dc–dc converter, power conversion system and its control, and reliability of power semiconductors.

JONG-WON SHIN (Senior Member, IEEE) received the B.S. and Ph.D. degrees in electrical engineering from Seoul National University, Seoul, South Korea, in 2006 and 2013, respectively. From 2013 to 2015, he was a Postdoctoral Researcher with Virginia Tech, Blacksburg, VA, USA. From 2015 to 2018, he was a Senior Scientist with the Electronics Research Department, Toyota Research Institute of North America, Ann Arbor, MI, USA. He was with Chung-Ang University, Seoul, as an Assistant Professor, from 2018 to 2022, and an Associate Professor, from 2022 to 2024. He joined Seoul National University, in 2024, where he is currently an Assistant Professor. From 2021 to 2024, he was a Visiting Associate Professor with Nagoya University, Nagoya, Japan. His research interests include power conversion, energy management, and power semiconductor packaging.

WONHEE KIM (Member, IEEE) received the B.S. and M.S. degrees in electrical and computer engineering and the Ph.D. degree in electrical engineering from Hanyang University, Seoul, South Korea, in 2003, 2005, and 2012, respectively.

From 2005 to 2007, he was with Samsung Electronics Company, Suwon, South Korea. In 2012, he was with the Power and Industrial Systems Research and Development Center, Hyosung Corporation, Seoul. In 2013, he was a Postdoctoral Researcher with the Institute of Nano Science and Technology, Hanyang University, and a Visiting Scholar with the Department of Mechanical Engineering, University of California at Berkeley, Berkeley, CA, USA. From 2014 to 2016, he was with the Department of Electrical Engineering, Dong-A University, Busan, South Korea. He is currently a Professor with the School of Energy Systems Engineering, Chung-Ang University, Seoul. His current research interests include nonlinear control and nonlinear observers and their industrial applications. He served as an Associate Editor for IEEE/ASME Transactions on Mechatronics, IEEE Access, and the *Journal of Electrical Engineering and Technology*.